# Tunable and switchable harmonic h-shaped pulse generation in a 3.03 km ultralong mode-locked thulium-doped fiber laser

JUNQING ZHAO,[1] LEI LI,[1] LUMING ZHAO,[1,*] DINGYUAN TANG,[1] DEYUAN SHEN,[1] AND LEI SU[2]

[1] *Jiangsu Key Laboratory of Advanced Laser Materials and Devices, Jiangsu Collaborative Innovation Center of Advanced Laser Technology and Emerging Industry, School of Physics and Electronic Engineering, Jiangsu Normal University, Xuzhou 221116, Jiangsu, China*
[2] *School of Engineering and Materials Science, Queen Mary University of London, London, UK*
**Corresponding author: lmzhao@ieee.org*

Received XX Month XXXX; revised XX Month, XXXX; accepted XX Month XXXX; posted XX Month XXXX (Doc. ID XXXXX); published XX Month XXXX

**We experimentally demonstrated a type of tunable and switchable harmonic h-shaped pulse generation in a thulium-doped fiber (TDF) laser passively mode-locked by using an ultra-long nonlinear optical loop mirror (NOLM). The total cavity length was ~3.03 km, the longest ever built for a TDF laser to our best knowledge, which resulted in an ultra-large anomalous dispersion over -200 ps$^2$ around the emission wavelength. The produced h-shaped pulse could operate either in a fundamental or in a high-order harmonic mode-locking (HML) state depending on pump power and intra-cavity polarization state (PS). The pulse duration, no matter of the operation state, was tunable with pump power. However, pulse breaking and self-organizing occurred, resulting in high order HML, when the pump power increased above a threshold. At a fixed pump power, the order of HML was switchable from one to another by manipulating the PS. Switching from 8$^{th}$ up to 48$^{th}$ order of HML was achieved with a fixed pump power of ~4.15 W. Our results revealed the detailed evolution and switching characteristics of the HML and individual pulse envelope with respect to both the pump power and PS. We have also discussed in detail on the mechanisms of both the h-shaped pulse generation and the switching of its HML. This contribution would be helpful for further in-depth study on the underlain dynamics of long duration, particular-envelope pulses with ultra-large anomalous dispersion and ultra-long roundtrip time.** 

http://dx.doi.org/10.1364/PRJ.99.099999

## 1. INTRODUCTION

Mode-locked fiber lasers, especially those passively mode locked by employing saturable absorbers, have attracted intensive investigation in recent years mainly motivated by two aspects. One was that some novel materials exhibiting saturable absorption continuously emerged and gained extensive attention, such as graphene [1-5], topological insulator [6-8], black phosphorus [9-12], MXene [13], etc. The other was attributed to the rich phenomena and dynamics relating to the passive mode-locking in fiber lasers, besides some typical solitons, that are still deserved to reveal or further investigate, like bunched multiple-soliton [7], vector solitons [11], bound-sate solitons [12], soliton rains [14], soliton molecules [15], dark pulses [16], dissipative soliton resonances [17, 18], etc.

Most investigations have devoted to fundamental mode-locking (FML), which produces a single pulse in one cavity roundtrip, resulting in a pulse repetition frequency (PRF) directly defined by the cavity length. FML represents the standard mode-locked operation of lasers that exhibits the highest stability. Besides that, harmonic mode-locking (HML) is a particular multiple-pulse phenomenon that exhibits equal pulse interval among adjacent pulses, i.e. the multiple pulses occupy the cavity uniformly through self-rearrangement, resulting in a state of operation at a multiple of the cavity-length-determined fundamental PRF. It has been considered as an attractive route to enhance the PRF of a passively mode-locked fiber laser in an integral multiple manner, through intense pumping and appropriate setting of the cavity-related parameters.

HML has been achieved in various mode-locking regimes, like solitons [19-22], bound-state solitons [23], twin-pulse solitons [24], soliton bunches [25], dissipative solitons [26, 27], dissipative soliton resonances (DSR) [28, 29], dark pulses [30-32], etc. Relying on wave-breaking-free properties attributed to peak-power-clamping (PPC) effect, DSR has recently been shown as a promising mode-locking regime that could scale the pulse energy to virtually unlimited levels,

and, in fact, up to 10 μJ single pulse energy from a fiber laser oscillator was achieved by G. Semaan et al [33]. The detailed amplifying characteristics of DSR pulses at 2 μm band were investigated by J. Zhao et al, where over 94 μJ amplified pulse energy was obtained with up to ~18.4 kW peak power from a thulium-doped fiber (TDF) master oscillator power amplifier (MOPA) system [34]. However, despite the unparalleled scalability in single pulse energy, the HML was still observed in the DSR regime [28, 29, 35]. It is suspected that the initial condition causes the HML [36], or the pulse energy limiting effect might be induced with some specific settings in the cavity, like the polarization state, the spectral-filtering effect, etc.

The most intensively investigated DSR pulses exhibit a well-known square wave or rectangular shape. The DSR pulses can form in both normal and anomalous dispersion regimes. However, due to soliton effects (pulse energy limiting, soliton splitting, etc.) some noise-like square wave pulses can also be easily produced from a fiber oscillator. Even if sharing similar pulse shape, the noise-like square wave pulses are quite different from typical DSR pulses. Although a noise-like square wave pulse looks like a single pulse from an oscilloscope with slow responded photodetector, a measurement by using an autocorrelator showed that it contained some fine structures on the square long envelop [37].

Besides the DSR pulse exhibiting square wave envelope, some other related pulse envelopes have also been observed, such as that with a tilt-top [38, 39]. For some other particular pulses, although they, strictly speaking, could not be identified as in the DSR regime, there were some similarities between them and the DSR pulse in envelop, like the chair-like pulses [40], step-like pulses [41], etc. Very recently, we observed another particular type of h-shaped pulse [42]. It had a narrow leading edge, similar to a sharp peak, and, meanwhile, showed some similar behaviors on its trailing portion with the DSR pulse, mainly including the well-known PPC effect and pump-power-dependent duration. As what has just been confirmed by H. Luo et al most recently [43], this type of pulse also shared some advantages of DSR pulse favorable by gain-switching, such as long-enough pump dependent pulse duration, freedom from wave-breaking, high pulse energy, etc. They achieved ~0.79 μJ of pulse energy at 2.103 μm with a repetition rate of 1.435 MHz from a holmium-doped fiber laser gain-switched by a TDF MOPA seeded with an h-shaped pulse source that they built. The built fiber laser cavity was ~137.2 m, and the achieved pulse duration was in several nanoseconds.

Although some single h-shaped pulse characteristics have been investigated experimentally in TDF lasers, there is still no investigation the related HML. There should be some possibility that an HML state of the h-shaped pulses might exist under some specific cavity designs and operation conditions, considering the observed similarities between the h-shaped and DSR pulses. In this paper, we demonstrated that tunable and switchable HML of h-shaped pulses were indeed able to be achieved if the cavity length was long enough, with some controllable conditions. In detail, we built a TDF laser resonator reaching ~3.03 km with an ultra-large anomalous dispersion over -200 $ps^2$ around the emission wavelength, which should be the longest cavity and the largest dispersion for a TDF laser ever built up to now, to the best of our knowledge. We also further investigated on the related evolution and switching characteristics with respect to the pump power and polarization state (PS), respectively.

## 2. EXPERIMENTAL SETUP

Figure 1 schematically shows the employed experimental layout. The fiber laser resonator was constructed with a typical figure-eight (f-8) configuration. The pump source was a compact all-fiber MOPA system including a single-frequency, wavelength-tunable, distributed feedback laser diode (DFB-LD), and an erbium-ytterbium fiber amplifier (EYFA). To enhance the pump absorption, the emission wavelength of the MOPA system should be as long as possible toward the peak absorption of the TDF in 1.6-1.7 μm region. For that, the peak wavelength of the seeding DFB-LD was tuned to its long-wavelength limit of ~1570.4 nm with ~5.3 mW continuous wave (CW) output power. The whole MOPA system could provide CW and nearly single-frequency output power continuously tunable from less than 100 mW to over 4 W at ~1570.4 nm.

Through a filter wavelength division multiplexer (FWDM), the pump light was coupled into a piece of TDF with a length of only ~16 cm. The TDF exhibits a specified core absorption of ~500 dB/m at 793 nm, core numerical aperture (NA) of 0.15, and core/cladding diameters of 10/130 μm, respectively. We used 82% port of an 18/82 fiber optical coupler (FOC) as the output for achieving high enough output power. To enable the unidirectional propagation of the produced signal laser in the gain fiber, an isolator was used at the other side of the FWDM. Through a 20/80 FOC, an asymmetric nonlinear optical loop mirror (NOLM) was constructed, in which a fiber spool with ~3.021 km long SMF-28e fiber was incorporated to lengthen the cavity and enhance the cumulative nonlinearity. Without any isolation, the split laser beams propagated bidirectionally in the NOLM, and then underwent an interference at the FOC. Two manual fiber polarization controllers (FPCs), one being 3-paddle type and the other in-line type, were incorporated into the fiber laser resonator to manipulate the intra-cavity PS. For the 3-paddle FPC used in the gain fiber loop, i.e., FPC-1, its 3 paddles consist 4, 8, and 4 loops of SMF-28e in series, with the same loop diameter of ~56 mm. Correspondingly, they roughly create a quarter-wave plate, a half-wave plate, and a quarter-wave plate, respectively. For the in-line FPC incorporated in the NOLM, i.e., FPC-2, the induced retardance can be tuned by adjusting the pressure and rotating the fiber squeezer.

The total geometrical length of the constructed fiber laser cavity was ~3.03 km. Apart from the ~16 cm TDF, all the used fiber pieces were Corning SMF-28e, which has a large value of anomalous dispersion around 2 μm band. This resulted in an ultra-large anomalous dispersion over -200 $ps^2$ estimated at the emission wavelength.

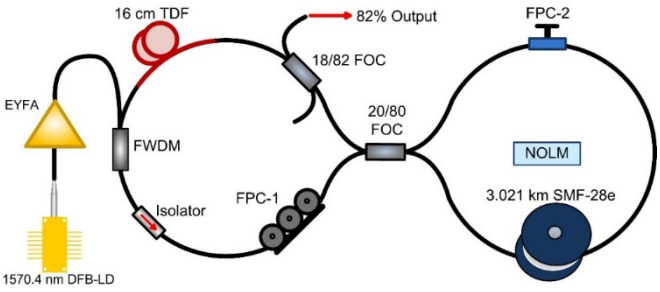


**Fig. 1.** Experimental layout.

## 3. RESULTS AND DISCUSSION

When the pump power increased to ~1.46 W, CW lasing started. The pumping threshold is ~1.58 W for stable, FML operation that could deliver single h-shaped pulse when the two FPCs were adjusted to appropriate orientations. Due to the ultra-large length of the fiber laser resonator, the generated pulse train exhibited an ultra-long repetition period of ~14.88 μs, which was also the cavity roundtrip time and corresponded to an ultra-low PRF of ~67.22 kHz. This indicates that FML with single h-shaped pulse emission was still possible even when the laser cavity reaches several kilometers long. HML emission could be observed with further increasing the pump power above a threshold value, when orientations of the two FPCs were fixed, i.e. the intra-cavity PS was locked to a particular one. We further observed

that both the pump power and intra-cavity PS could considerably affect the characteristics of the h-shaped pulse trains as well as each individual pulse. Below, we will discuss these output characteristics in details.

### A. Pump-power-related switching and evolution

Figure 2 shows the detailed switching characteristics from the FML to some higher orders of HML with the pump power increasing. The left figures (a)-(e) show several captured temporal traces with the same span, covering two repetition periods, i.e., two cavity roundtrips. It can be seen that all the temporal traces, no matter of the FML or the different orders of HML, contained pulses with distinctly h-shaped envelops. With ~4.15 W pump power, the maximum pump power we utilized here, and the same fixed PS, up to 8th order of HML could be achieved, as seen from the pulse train shown in Fig. 2(e). It should be noted that all these pulse trains were recorded under identical conditions. All the temporal characteristics throughout this paper were measured by using a 2 μm InGaAs photodetector (PD, ET-5000, Electro-Optics Technology, Inc.) in combination with a real time digital storage oscilloscope (DSO, DSO9104A, Agilent Technologies, Inc.). As specified, the PD has a bandwidth (BW) of >12.5 GHz and rise/fall time of 28ps. The DSO exhibits a maximum sampling rate of 20 GSa/s, a typical rise/fall time of 253 ps (10-90%), and a BW of 1 GHz. Considering the large recording temporal length along with too much time required, here we used a sampling rate of 5 GSa/s to record the pulse trains, rather than the maximum value.

Figures 2(f) through 2(j) recorded several captured radio frequency (RF) traces corresponding to the left side temporal traces, which were directly detected by using the same photodetector, but were further recorded by using an RF spectrum analyzer (N9320B, Agilent Technologies, Inc.). Here, the recording span was 10 MHz with a resolution BW (RBW) of 100 Hz. For each trace, despite the comb-like frequency lines determined by the PRF, the large-scale modulation pattern across them was resulted from the long temporal duration of the lower part of each h-shaped pulse. Mathematically, the modulation frequency and that temporal duration satisfied a reciprocal relationship.

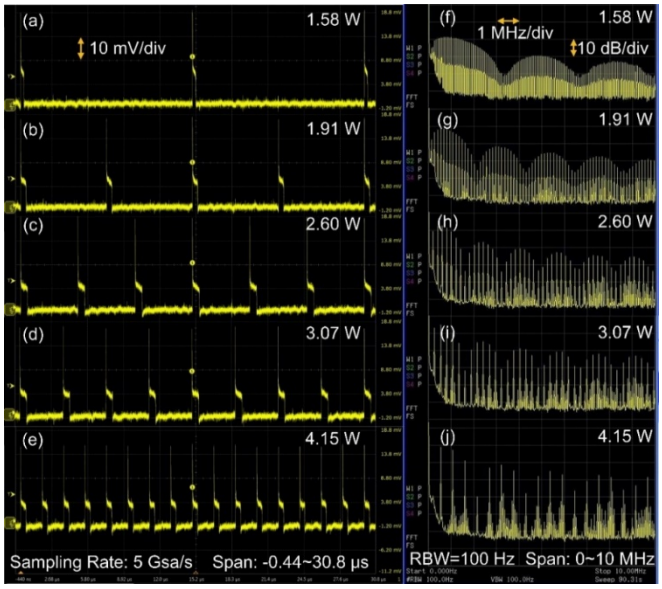


**Fig. 2.** Pump power induced harmonic switching with the (a-e) pulse trains [(a) through (e)] and RF spectra [(f) through (j)].

Figure 3 plots the spectral profiles corresponding to the h-shaped pulses shown in Fig. 2, measured by using a long wavelength optical spectrum analyzer (OSA, AQ6375B, Yokogawa Test & Measurement Co.) with a setting resolution of 0.05 nm. As seen, the highly structured spectral profiles, especially the pronounced sharp cuts distributing across them, were mainly caused by the absorption lines of atmospheric molecules, primarily of water [44]. Despite the structured profiles, we could still roughly discern the spectral evolution with pump power. One was that the higher the pump power, the broader the spectra spanned. The second was that there was a minor redshift on the peak wavelength, i.e. ~1846.42 to ~1850.18 nm as the pump power increasing from ~1.58 up to ~4.15 W.

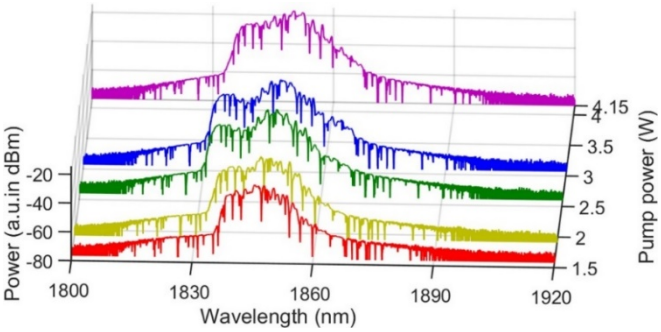


**Fig. 3.** Output optical spectra with different pump powers, also corresponding to different orders of HML.

In a fixed PS and before the laser switched from one state to another one, temporal characteristics of the output pulse could be continuously varied with the pump power. Figure 4 plots several pulse envelop with different pump powers when the TDF laser operated with FML. The lower-part pulse duration, estimated at half the amplitude of the trailing edge, extended from ~180 ns to ~410 ns as the pump power increased from ~1.58 to ~1.78 W, which was similar to the temporal characteristics of fiber lasers working in typical DSR regime [17, 18]. As could be seen, each pulse exhibited a sharp leading peak and a followed flat trailing portion, more clearly showing an "h"-like shape. Another noticeable characteristic was that the trailing portion remained roughly unchanged with the pump power. This was also quite similar to the case of DSR regime. These temporal characteristics of the flat trailing portion were just due to the PPC effect.

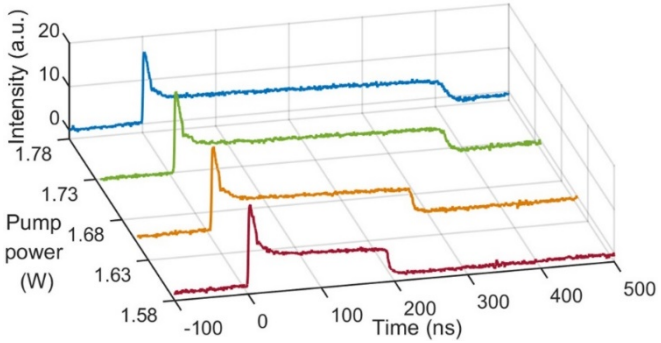


**Fig. 4.** Pump power induced evolution with the single pulse envelop when the TDF laser operated with fundamental repetition rate.

In addition, it should be noted that the trailing portion was not resulted from amplified spontaneous emission (ASE), although some similarities might be shared. In a fiber amplifier with ultra-low repetitive seeding pulses (typically less than tens of kHz), ASE can arise if the pump is continuous. In our fiber laser, however, the PRF was high enough, especially with the HML, which was not so easy to induce

significant ASE in the pulse intervals. Moreover, compared to the single-pass fiber amplifier, the oscillating characteristics of the fiber laser could also provide some suppression on the ASE.

These evolution characteristics are consistent with our previous observations in Ref. [42], but no HML was observed there. These observations indicate that the h-shaped pulse formation is partially resulted from the PPC effect. This effect flatten the long trailing portion and prevent the pulse splitting, no matter it is with the FML or HML state. However, we are so far not sure about how the sharp leading part of the h-shaped pulse is generated. The HML of the h-shaped pulses, as a particular multiple pulse phenomenon, is due to the too much strong pump power and limited pulse energy. Then due to the self-rearrangement process in the fiber laser, the multiple pulses can occupy the cavity in a uniform manner, finally resulting the HML formation.

### B. PS-induced switching characteristics

Besides the pump power related evolution and switching characteristics of the h-shaped pulses in FML and HML, another interesting issue is whether the PS can affect the operating state of the TDF laser. To confirm it, we then conducted an experiment, in which the intra-cavity PS was manipulated through adjusting the two FPCs while the output characteristics were monitored simultaneously. It was then verified that, although our cavity length reached several kilometers, the achievable pulse energy was still highly influenced by the intra-cavity PS, which resulted in the PS-dependences of the HML.

The HML could be switched from 8$^{th}$ up to 48$^{th}$ order by simply manipulating the PS when the pump power was fixed at ~ 4.15 W. Figure 5 shows several captured pulse trains for some of those different orders of HML. It could be seen that as the HML switching from a lower to a higher order, the peak intensity lowered down rapidly, and the duration of the trailing portion narrowed down, from ~491 ns to ~85 ns. However, no significant change on the intensity of the trailing portion could be observed.

The 48$^{th}$ order of HML is the highest one we can achieve presently. Although much higher orders of HML have been observed and reported in other ultrashort soliton mode-locking regimes [45, 46], HML of h-shaped pulses with high order would encounter one intrinsic problem. As what we know, the ultrashort soliton operations typically exhibit an extremely large pulse interval in contrast to its ultrashort pulse duration, which results in a tiny pulse duty circle (PDC). Due to the basic limitation in soliton energy according to the well-known area-theorem, soliton is very readily to split under intensive pump, especially in an ultra-long cavity and all-anomalous-dispersion regime. That is why soliton operation can easily reach a high order of HML. For the h-shaped pulse, however, it typically has a long duration evaluated by considering the trailing portion if an ultra-long cavity is employed and an intensive pump is applied. For our case, the achieved longest duration reached over 600 ns [Fig. 2(c)], which was $10^6$ (one million) times longer than typical soliton pulses. This means that, for an identical condition, the h-shaped pulses could have a PDC several orders higher than that of typical solitons. Thus, for too high an order of HML, the long trailing portion of the h-shaped pulses would fully occupy the pulse intervals, i.e., adjacent pulses would nearly overlap with each other. In the experimental aspect, however, the pulses would typically merge into a continuous wave operation rather than forming a pulse overlap state, like what we observed in our previous publication where the PDC could approach to 98.2% but its further increase would result in the transformation into a continuous wave state [34].

Besides the intrinsic issue, other factors on the limitation of the highest order of HML, i.e, 48$^{th}$ order here, mainly included the available pump power, the large attenuation loss of silica fibers at 2 μm band, and especially the hindering on pulse splitting due to the PPC effect that we have discussed at the end of subsection **3 A**. If we consider some other approaches like utilizing the acoustic stabilization effect adopted in Refs. [45, 46], higher orders of pulses might be possible, but it cannot ensure that the laser would still be able to operate in the h-shaped pulse regime then.

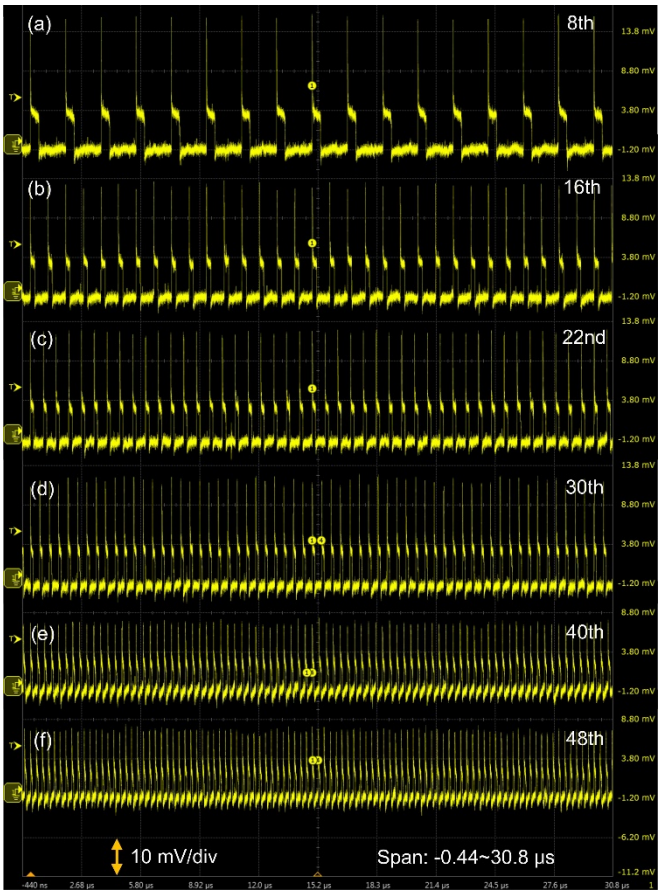


**Fig. 5.** Several pulse trains with different orders of HML switched by PS-manipulation with a fixed pump power of ~4.15 W.

We have also tried to measure autocorrelation trace of the h-shaped pulse to confirm if there were some fine structures or noise-like tiny pulses hidden in the long pulse packet. No matter how we varied the pump power and manipulated the PS, there was no noticeable short trace could be observed within the maximum span of our available autocorrelator (APE, Angewandte Physik & Elektronik GmbH, PulseCheck). We prefer that there are no fine structures or noise-like pulses hidden in the trailing portion of the h-shaped packet, although further experimental evidence is required for this claim.

Supermodes can typically be produced in an HML fiber laser [19]. In the HML operation of the h-shaped pulses, we also observed the supermodes along with the main PRF lines, as seen from the RF traces in Fig. 6 that were recorded with an RBW of 10 Hz and a span of 0~4 MHz. Only clean RF lines could be observed with the FML, as seen in Fig. 6(a). However, supermode lines appeared between the main PRF lines, once the laser switching to an HML state either by increasing the pump power or by manipulating the PS. The higher the order of HML was, the stronger the generated supermodes, i.e., the lower the supermode suppression ratio (SMSR), was observed. Taking the 16$^{th}$ order of HML for instance, as seen in Fig. 6(e), the SMSR was ~38.6 dB, whereas it decreased to ~12.8 dB when the HML reached 48$^{th}$ order [Fig. 6(h)].

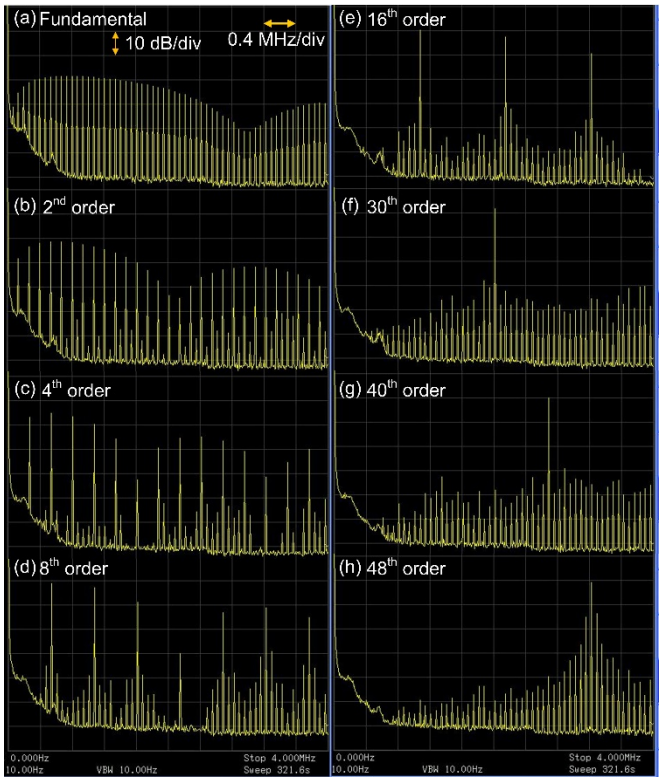


**Fig. 6.** Detailed RF characteristics with the FML [(a)] and different orders of HML [(b) through (h)].

Besides the PS-tuning could effectively enable the HML-order switching, it was noticed that specific FPC location could also exert some influences on the temporal characteristics. The switching characteristics relating to both the PS-tuning and FPC-location could be understood as follows.

In principle, adjusting the paddle(s) or fiber squeezer of an FPC will vary the local fiber birefringence, which results in the change on the induced phase retardance. For FPC-1, if it was placed prior to the TDF, the induced retardance would experience some amplification due to the fiber gain compared to where it was placed after the TDF, as in Fig. 1. However, no matter where it was placed, it seemed no significant difference on the transmittance of the NOLM would be induced by its specific location because of the unidirectional propagation enabled by the isolator. Alternatively, rotating any paddle of FPC-1, in any case, could vary the output pulse characteristics considerably, which was probably due to the resulted change on the total cavity birefringence, similar to the case we observed in our previous publication [42]. In detail, although the FPC-1 did not directly vary the transmittance of the NOLM, it could vary the overall cavity birefringence by inducing some additional amount of fiber birefringence. This further resulted the change on the PS of the input pulse to the NOLM, i.e., altering the coupling between the two orthogonal field components of the pulse. This could induce a different nonlinear phase retardance $\Delta\phi_{NL}$ within the NOLM, corresponding to a change of the transmittance of the NOLM. Thus, the FPC-1 could vary the transmittance of the NOLM in an indirect manner, but somehow it could influence the output pulse characteristics considerably.

For FPC-2, however, we noticed that its specific location could indeed affect the output pulse characteristics. Most noticeably, placing FPC-2 near to the 80% port of the FOC could vary the pulse characteristics much more dramatically than placing it near to the 20% port, where we have assumed that the input was provided by the port connecting FPC-1. The probable reason might be understood from the resulted different transmittances of the NOLM with these two locations. The details can be analyzed as follows.

The pulse peak power from the 80% port is higher than that from the 20% port, which experiences a larger nonlinear phase shift $\phi_{NL}$ comparatively in the NOLM. $\phi_{NL}$ can be calculated by using the formula [47],

$$\phi_{NL} = \frac{2\pi n_2}{\lambda A_{eff}} P_0 L_{eff}. \quad \textbf{(1)}$$

$n_2$ is the nonlinear-index coefficient, $\lambda$ is the light wavelength in vacuum, $A_{eff}$ is the effective mode area of the fiber (here SMF-28e), $P_0$ is the pulse peak power, and $L_{eff}$ is the effective propagation. $L_{eff}$ is approximately the length of the NOLM by neglecting its loss. Except $P_0$, all other parameters in Eq. (1) can be considered as constant values. Thus, if the peak power difference between the counter-propagating pulses in the NOLM is noted as $\Delta P$, the resulted phase retardance $\Delta\phi_{NL}$ between the two beams, when they arrive at the FOC again after counter-propagating through the NOLM, is

$$\Delta\phi_{NL} = \frac{2\pi n_2 L_{eff}}{\lambda A_{eff}} \Delta P = (1-2\alpha)\frac{2\pi n_2 L_{eff}}{\lambda A_{eff}} P_{in}. \quad \textbf{(2)}$$

$P_{in}$ is the input pulse peak power of the NOLM. In Eq. (2), we have related $\Delta P$ with $P_{in}$ as $\Delta P = (1-2\alpha)P_{in}$, with $\alpha$ being splitting ratio of the FOC (here $\alpha = 0.2$).

With no other retardance, the transmittance $T$ of the NOLM will be determined solely by $\Delta\phi_{NL}$ as the following relationship [48],

$$T = 1 - 2\alpha(1-\alpha)[1 + cos(\Delta\phi_{NL})]. \quad \textbf{(3)}$$

However, if FPC-2 is tuned to produce an additional retardance, noted as $\Delta\phi_{FPC}$, $T$ will be changed. Moreover, $T$ is dependent on the location of FPC in the NOLM, and roughly satisfies

$$T = 1 - 2\alpha(1-\alpha)[1 + cos(\Delta\phi_{NL} \pm \Delta\phi_{FPC})]. \quad \textbf{(4)}$$

If FPC-2 is placed near to the 80% port of the FOC, +sign should be chosen. Otherwise, –sign should be chosen if it is placed near to the 20% port. Further taking a derivative of $T$ with respect to $(\Delta\phi_{NL} \pm \Delta\phi_{FPC})$, we obtain

$$\frac{dT}{d(\Delta\phi_{NL} \pm \Delta\phi_{FPC})} = 2\alpha(1-\alpha)sin(\Delta\phi_{NL} \pm \Delta\phi_{FPC}) \quad \textbf{(5)}$$

For the FML, the pulse peak power is roughly three times the power of the flat trailing portion, as shown in Fig. 5(a), which can be roughly calculated as ~1.25 W. Based on Eq. (2), $\Delta\phi_{NL} \approx 4.003\ rad$ through calculation. Substituting this value into Eq. (5), it can be seen that, compared to the resulted value without $\Delta\phi_{FPC}$, a larger rate of change on $T$ would be induced for a small positive value of $\Delta\phi_{FPC}$; conversely, a smaller one would be induced for a small but negative value of $\Delta\phi_{FPC}$. Thus, it would be easier to obtain a more dramatic change on the pulse characteristics if FPC-2 is placed near to the 80% port comparatively. In fact, we have placed it there, as shown in Fig. 1, for achieving as many HML states as possible from the FML through tuning the FPC-2.

From Eqs. (4) and (5), no matter the location of FPC-2, i.e., no matter + or – sign might be chosen, $\Delta\phi_{FPC}$ could induce some change on the transmittance of the NOLM, which could further vary the overall characteristics of the mode-locking. Most significantly, this could induce the HML-order switching. Certainly, the FPC-2 might also be placed at other locations in the NOLM. According to Eqs. (4) and (5), some intermediate tuning effects might be achievable compared to the two extreme cases just discussed.

Despite the FPC-related switching characteristics of the HML, we further noticed that when the pump power was too high, it was impossible to obtain the FML no matter how the two FPCs were adjusted. Taking the ~4.15 W pump power for instance, the obtainable lowest order of HML was 8th. This indicated that the h-shaped pulse could not be a type of energy-unlimited pulse under some extreme conditions, like the ultra-large length of the cavity here. In a more in-depth way, with high-enough pump power, strong-enough

nonlinearity and large-enough dispersion, the prevention of pulse-splitting effect of the h-shaped pulse became impossible through typical approaches, such as the PS manipulation.

As a short summary, the switching of HML could be achieved by two methods: one is to simply vary the pump power with fixed PS; the other one is to change the PS with fixed pump power. The former one is achieved due to the limited PPC effect. Consequently, the varying pump power will change the pulse number. The latter one is achieved by changing the supported pulse energy, hence the pulse number changes as the total output power is nearly maintained.

### C. Other HML-order-related characteristics

To further understand the possible mechanisms behind the HML of h-shaped pulses, it should also be helpful to compare the detailed characteristics of each individual pulse with pump-power-related different orders of HML. We then plotted them as shown in Fig. 7. As can be seen, both the leading and trailing portions of each h-shaped pulse decreased as it splitting into more pulses with higher order of HML, which was achieved by increasing the pump power. This might indicate that it should be the pulse splitting altered the PPC effect, rather than that the latter induced the former. Thus, although the clamped peak powers exhibited some changes for different orders of HML, the PPC effect should still be able to shape the h-shaped pulses (at least on the trailing portions), both with the FML as what we claimed in Ref. [42] and HML here. However, the PPC effect should not be the cause for HML. In fact, the PPC effect could somehow hinder the laser developing into a higher order HML by preventing the pulse breaking or splitting. HML of the h-shaped pulse might be due to other factors, such as the nonlinearity, birefringence, spectral-filtering, as well as other higher order (over the 2nd order) effects, although it is currently still beyond our ability to reach an exact conclusion on which one or even which combination of several of them dominated this phenomenon. These factors caused some limitation on the PPC effect, which further resulted the pulse breaking, i.e., the laser being switched to a higher order of HML.

From Fig. 7, it could also be noticed that the duration of the flat trailing portion was not linear or at least not monotonic to the pump power, which was caused by the switching among different orders of HML. The details are as follows. It was found that, only with the same order of HML or with the FML, the pulse peak power could be clamped to a certain value, and the duration of the pulse trailing portion would increase almost linearly to the pump power. Once being switched to another different order of HML, however, the pulse duration would experience a sudden change due to the pulse splitting or merging, and then the new pulse envelop would follow a linear evolution again with the pump power, until next switching on the HML-order. Because both the trailing duration immediately after a splitting or merging and the further broadening in duration due to the PPC effect might be different, the recorded trailing duration did not follow a monotonic evolution with respect to the HML order.

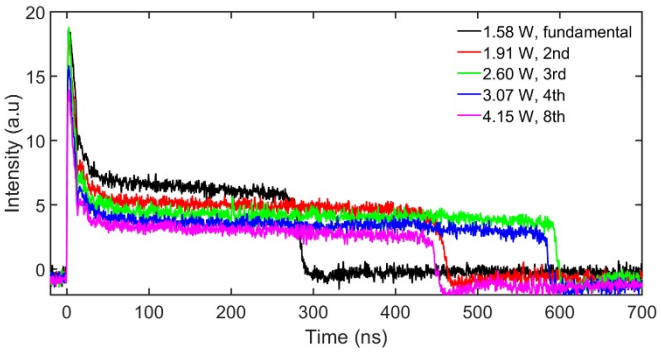


**Fig. 7.** Detailed pulse envelope of each individual h-shaped pulse with PS-fixed, pump-power-related, different orders of HML.

Another interesting issue was how the pulse peak duration might vary with the pump power and HML-order. Although the responses of both the available photodetector and oscilloscope were limited, they should be able to give some rough measurements considering that the pulse peak durations were in the nanosecond range (as previously mentioned, the autocorrelation measurement can not be used to confirm if there were some ultrashort fine structures embedded). The measured results were shown in Fig. 8.

As illustrated in the inset of Fig. 8(a), the pulse peak duration was evaluated at the points on the pulse envelop where the power $P_{1/2,peak}$ related to the sharp peak leading power $P_{leading}$ and the trailing portion power $P_{trailing}$ as

$$P_{1/2,peak} = P_{trailing} + \frac{1}{2}\left(P_{leading} - P_{trailing}\right) = \frac{1}{2}\left(P_{leading} + P_{trailing}\right) \quad (6)$$

Figure 8(a) plots its evolution with the pump power. As seen, it narrowed down as the pump power increasing with the FML, although the trailing portion broadened in this process as seen in Fig. 4. As also be noticed, narrowing down also occurred with the pulse switching to some higher order of HML. Much differently by PS-tuning, however, the pulse peak duration increased with the HML switching into to a higher order when the pump power was fixed to ~4.15 W, as seen in Fig. 8(b). The difference might be understood by comparing Figs. 2 and 5. In Fig. 2, it could be noticed that although the laser transformed into to some higher orders of HML as the pump power increasing above the related threshold values, no much lowering in the pulse peak power could be observed. Thus, it could be intuitively deduced that the pulse duration narrowing was possible considering the process with a pulse abruptly breaking into more pulses with similar peak powers. From Fig .5, however, much more significant lowering in pulse peak power could be observed. Thus, the evaluation points on the pulse peak duration would be much closer to the trailing portion, i.e., $P_{1/2,peak} \to P_{trailing}$, which would make the evaluated peak duration longer. This might be why we could observe the peak duration increasing with the HML-order, in Fig. 8(b), when we tuned the two FPCs without varying the pump power.

Although the plots showed some differences in Figs. 8(a) and 8(b), they all followed some monotonic trends, which were quite different from the characteristics of trailing portion shown in Fig. 7. This further indicated that the peak leading portion might be at least incompletely clamped, and the PPC effect was quite weak or even negligible in shaping the sharp peak. Thus, this portion should follow evolutions similar to other typical pulses without PPC effect.

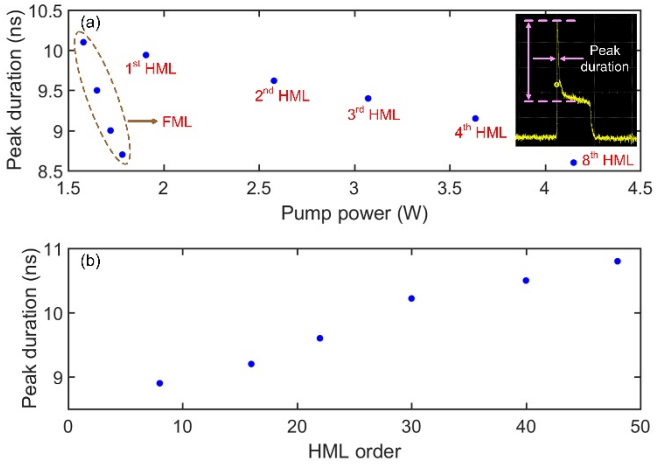


**Fig. 8.** The evolutions of pulse peak duration with respect to the (a) pump power with a fixed PS, and (b) HML order with a fixed pump power, respectively.

For the PS-related different orders of HML, the emitted average output power also showed some PS dependences. As the plots in Fig. 9, all the power evolutions under different PSs showed roughly linear tendencies with the pump power. Moreover, from the calculated slope efficiencies, it could be seen that the higher the achieved order of HML, the higher the corresponding slope efficiency, i.e. the larger average output power. This indicated that a higher order of HML should be preferably achieved with a higher effective laser gain, and the effective laser gain should be partially determined by the intra-cavity PS.

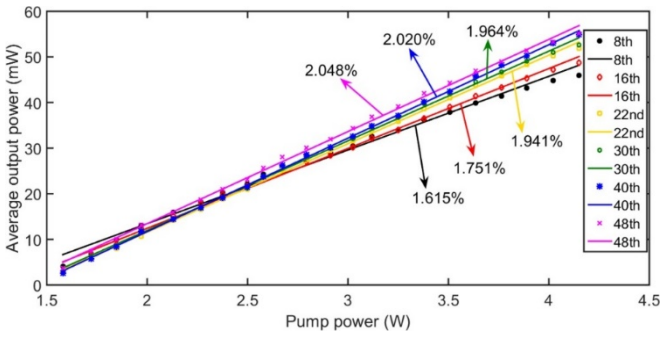


**Fig. 9.** Average output power versus pump power for PS-induced different orders of HML.

## 4. CONCLUSION

In conclusion, we have experimentally investigated on the HML characteristics of a type of h-shaped pulses produced in an NOLM-mode-locked TDF laser with ultra-long cavity as well as ultra-large anomalous dispersion. Both the pump power and PS related evolution and switching behaviors were observed in the HML. For each individual pulse, pump power induced broadening occurred no matter with the FML or with some higher order of HML. Further discussions and analyses were also given on the related mechanisms with those experimental observations. Our results experimentally verified that single h-shaped pulse could exist even in kilometers long fiber laser resonator, and its HML could be achieved and switched through appropriate manipulations of the pump power and intra-cavity PS.

**Funding.** Natural Science Foundation of Jiangsu Province (BK20170243), National Natural Science Foundation of China (NSFC) (61705094, 11674133, 11711530208, 61575089), Key Research Program of Natural Science of Jiangsu Higher Education Institutions (17KJA416004), Royal Society (IE161214); Protocol of the 37th Session of China-Poland Scientific and Technological Cooperation Committee (37-17). This project has received funding from the European Union's Horizon 2020 research and innovation programme under the Marie Skłodowska-Curie grant agreement No. 790666.

**Acknowledgment**. We acknowledge support from Jiangsu Overseas Visiting Scholar Program for University Prominent Young & Middle-aged Techers and Presidents; Priority Academic Program Development of Jiangsu Higher Education Institutions (PAPD).

## References

1. Q. Bao, H. Zhang, Y. Wang, Z. Ni, Y. Yan, Z. X. Shen, K. P. Loh, D. Y. Tang, "Atomic-layer graphene as a saturable absorber for ultrafast pulsed lasers," Adv. Funct. Mater. **19**, 3077 (2009).
2. H. Zhang, Q. Bao, D. Tang, L. Zhao, and K. Loh, "Large energy soliton erbium-doped fiber laser with a graphene-polymer composite mode locker," Appl. Phys. Lett. **95**, 141103 (2009).
3. H. Zhang, D. Y. Tang, L. M. Zhao, Q. L. Bao, and K. P. Loh, "Large energy mode locking of an erbium-doped fiber laser with atomic layer graphene," Opt. Express **17**, 17630 (2009).
4. Z. Sun, T. Hasan, F. Torrisi, D. Popa, G. Privitera, F. Wang, F. Bonaccorso, D. M. Basko, and A. C. Ferrari, "Graphene mode-locked ultrafast laser," ACS Nano, **4**, 803 (2010).
5. Z. Sun, D. Popa, T. Hasan, F. Torrisi, F. Wang, E. J. R. Kelleher, J. C. Travers, V. Nicolosi, and A. C. Ferrari, "A stable, wideband tunable, near transform-limited, graphene-mode-locked, ultrafast laser," Nano Res. **3**, 653 (2010).
6. C. Zhao, Y. Zou, Y. Chen, Z. Wang, S. Lu, H. Zhang, S. Wen, and Dingyuan Tang, "Wavelength-tunable picosecond soliton fiber laser with Topological Insulator: Bi2Se3 as a mode locker," Opt. Express **20**, 27888 (2012).
7. Y. Chen, M. Wu, P. Tang, S. Chen, J. Du, G. Jiang, Y. Li, C. Zhao, H. Zhang, and S. Wen, "The formation of various multi-soliton patterns and noise-like pulse in a fiber laser passively mode-locked by a topological insulator based saturable absorber," Laser Phys. Lett. **11**, 055101 (2014).
8. P. Yan, R. Lin, H. Chen, H. Zhang, A. Liu, H. Yang, and S. Ruan, "Topological insulator solution filled in photonic crystal fiber for passive mode-locked fiber laser," IEEE Photon. Technol. Lett. **27**, 264 (2015).
9. Y. Chen, G. Jiang, S. Chen, Z. Guo, X. Yu, C. Zhao, H. Zhang, Q. Bao, S. Wen, D. Tang, and D. Fan, "Mechanically exfoliated black phosphorus as a new saturable absorber for both Q-switching and Mode-locking laser operation," Opt. Express **23**, 12823 (2015).
10. Z. Luo, M. Liu, Z. Guo, X. Jiang, A. Luo, C. Zhao, X. Yu, W. Xu, and H. Zhang, "Microfiber-based few-layer black phosphorus saturable absorber for ultra-fast fiber laser," Opt. Express **23**, 20030 (2015).
11. Y. Song, S. Chen, Q. Zhang, L. Li, L. Zhao, H. Zhang, and D. Tang, "Vector soliton fiber laser passively mode locked by few layer black phosphorus-based optical saturable absorber," Opt. Express **24**, 25933 (2016).
12. Z. Wang, Y. Xu, S. C. Dhanabalan, J. Sophia, C. Zhao, C. Xu, Y. Xiang, J. Li, and H. Zhang, "Black phosphorus quantum dots as an efficient saturable absorber for bound soliton operation in an erbium doped fiber laser," IEEE Photon. J. **8**, 1503310 (2016).
13. X. Jiang, S. Liu, W. Liang, S. Luo, Z. He, Y. Ge, H. Wang, R. Cao, F. Zhang, Q. Wen, J. Li, Q. Bao, D. Fan, and H. Zhang, "Broadband nonlinear photonics in few-layer MXene $Ti_3C_2T_x$ (T = F, O, or OH)," Laser Photonics Rev. **12**, 1700229 (2018).
14. S. Chouli and P. Grelu, "Rains of solitons in a fiber laser," Opt. Express **17**, 11776 (2009).
15. X. Liu, X. Yao, and Y. Cui, "Real-time observation of the buildup of soliton molecules," Phys. Rev. Lett. **121**, 023905 (2018).
16. H. Zhang, D. Y. Tang, L. M. Zhao, and X. Wu, "Dark pulse emission of a fiber laser," Phys. Rev. A **80**, 045803 (2009).

17. W. Chang, A. Ankiewicz, J. M. Soto-Crespo, and N. Akhmediev, "Dissipative soliton resonances," Phys. Rev. A **78**, 023830 (2008).
18. X. Wu, D. Y. Tang, H. Zhang, and L. M. Zhao, "Dissipative soliton resonance in an all-normal-dispersion erbium-doped fiber laser," Opt. Express **17**, 5580 (2009).
19. C. Mou, R. Arif, A. Rozhin, and S. Turitsyn, "Passively harmonic mode locked erbium doped fiber soliton laser with carbon nanotubes based saturable absorber," Opt. Mater. Express **2**, 884 (2012).
20. J. Du, S. M. Zhang, H. F. Li, Y. C. Meng, X. L. Li, and Y. P. Hao, "L-band passively harmonic mode-locked fiber laser based on a graphene saturable absorber," Laser Phys. Lett. **9**, 896 (2012).
21. Z. Luo, M. Liu, H. Liu, X. Zheng, A. Luo, C. Zhao, H. Zhang, S. Wen, and W. Xu, "2 GHz passively harmonic mode-locked fiber laser by a microfiber-based topological insulator saturable absorber," Opt. Lett. **38**, 5212 (2013).
22. M. Liu, A. Luo, W. Xu, and Z. Luo, "Coexistence of bound soliton and harmonic mode-locking soliton in an ultrafast fiber laser based on MoS2-deposited microfiber photonic device," Chin. Opt. Lett. **16**, 020008 (2018).
23. Y. Wang, D. Mao, X. Gan, L. Han, C. Ma, T. Xi, Y. Zhang, W. Shang, S. Hua, and J. Zhao, "Harmonic mode locking of bound-state solitons fiber laser based on $MoS_2$ saturable absorber," Opt. Express **23**, 205 (2015).
24. B. Zhao, D. Y. Tang, P. Shum, W. S. Man, H. Y. Tam, Y. D. Gong, and C. Lu, "Passive harmonic mode locking of twin-pulse solitons in an erbium-doped fiber ring laser," Opt. Commun. **229**, 363 (2004).
25. L. M. Zhao, D. Y. Tang, T. H. Cheng, C. Lu, H. Y. Tam, X. Q. Fu, and S. C. Wen, "Passive harmonic mode locking of soliton bunches in a fiber ring laser," Opt. Quant. Electron. **40**, 1053 (2008).
26. L. M. Zhao, D. Y. Tang, T. H. Cheng, H. Y. Tam, and C. Lu, "Passive harmonic mode locking of gain-guided solitons in Erbium-doped fiber lasers," Chin. Sci. Bull. **53**, 676 (2008)
27. J. Peng, L. Zhan, S. Luo, and Q. Shen, "Passive harmonic mode-locking of dissipative solitons in a normal-dispersion Er-doped fiber laser," J. Lightwave Technol. **31**, 3009 (2013).
28. Y. Lyu, H. Shi, C. Wei, H. Li, J. Li, and Y. Liu, "Harmonic dissipative soliton resonance pulses in a fiber ring laser at different values of anomalous dispersion," Photon. Res. **5**, 612 (2017).
29. G. Semaan, A. Niang, M. Salhi, and F. Sanchez, "Harmonic dissipative soliton resonance square pulses in an anomalous dispersion passively mode-locked fiber ring laser," Laser Phys. Lett. **14**, 055401 (2017).
30. X. Li, S. Zhang, Y. Meng, and Y. Hao, "Harmonic mode locking counterparts of dark pulse and dark-bright pulse pairs," Opt. Express **21**, 8409 (2013).
31. J. Q. Zhao, Y. G. Wang, P. G. Yan, S. C. Ruan, G. L. Zhang, H. Q. Li, and Y. H. Tsang, "An L-band graphene-oxide mode-locked fiber laser delivering bright and dark pulses," Laser Phys. **23**, 075105 (2013).
32. R. Lin, Y. Wang, P. Yan, G. Zhang, J. Zhao, H. Li, S. Huang, G. Cao, and J. Duan, "Bright and dark square pulses generated from a graphene-oxide mode-locked ytterbium-doped fiber laser," IEEE Photon. J. **6**, 1500908 (2014).
33. G. Semaan, F. B. Braham, J. Fourmont, M. Salhi, F. Bahloul, and F. Sanchez, "10 μJ dissipative soliton resonance square pulse in a dual amplifier figure-of-eight double-clad Er:Yb mode-locked fiber laser," Opt. Lett., **41**, 4767 (2016).
34. J. Zhao, D. Ouyang, Z. Zheng, M. Liu, X. Ren, C. Li, S. Ruan, and W. Xie "100 W dissipative soliton resonances from a thulium-doped double-clad all-fiber-format MOPA system," Opt. Express, **24**, 12072 (2016).
35. C. Shang, X. Li, Z. Yang, S. Zhang, M. Han, J. Liu, "Harmonic dissipative soliton resonance in an Yb-doped fiber laser," J. Lightwave Technol. **36**, 4932 (2018).
36. A. Komarov, F. Amrani, A. Dmitriev, K. Komarov, and F. Sanchez, "Competition and coexistence of ultrashort pulses in passive mode-locked lasers under dissipative-soliton-resonance conditions," Phys. Rev. A, **87**, 023838 (2013).
37. J. Liu, Y. Chen, P. Tang, C. Xu, C. Zhao, H. Zhang, and S. Wen, "Generation and evolution of mode-locked noise-like square-wave pulses in a large-anomalous-dispersion Er-doped ring fiber laser," Opt. Express **23**, 6418 (2015).
38. J. Zhao, L. Li, L. Zhao, D. Tang, and D. Shen, "Dissipative soliton resonances in a mode-locked holmium-doped fiber laser," IEEE Photon. Technol. Lett. **30**, 1699 (2018).
39. L. Zhao, D. Li, L. Li, X. Wang, Y. Geng, D. Shen, and L. Su, "Route to larger pulse energy in ultrafast fiber lasers," IEEE J. Sel. Topics Quantum Electron. **24**, 8800409 (2018).
40. P. K. Gupta, C. P. Singh, A. Singh, S. K. Sharma, P. K. Mukhopadhyay, and K. S. Bindra, "Chair-like pulses in an all-normal dispersion Ytterbium-doped mode-locked fiber laser," Appl. Opt. **55**, 9961 (2016).
41. D. Mao, X. Liu, L. Wang, H. Lu, and L. Duan, "Dual-wavelength step-like pulses in an ultra-large negative-dispersion fiber laser," Opt. Express **19**, 3996 (2011).
42. J. Zhao, L. Li, L. Zhao, D. Tang, and D. Shen, "Cavity-birefringence-dependent h-shaped pulse generation in a thulium-holmium-doped fiber laser," Opt. Lett. **43**, 247 (2018).
43. Hongyu Luo, Fei Liu, Jianfeng Li, and Yong Liu, "High repetition rate gain-switched Ho-doped fiber laser at 2.103 μm pumped by h-shaped mode-locked Tm-doped fiber laser at 1.985 μm," Opt. Express **26**, 26485 (2018).
44. F. Haxsen, D. Wandt, U. Morgner, J. Neumann, and D. Kracht, "Monotonically chirped pulse evolution in an ultrashort pulse thulium-doped fiber laser," Opt. Lett. **37**, 1014 (2012).
45. M. S. Kang, N. Y. Joly, and P. St. J. Russell, "Passive mode-locking of fiber ring laser at the 337th harmonic using gigahertz acoustic core resonances," Opt. Lett. **38**, 561 (2013).
46. Q. Kuang, L. Zhan, Z. Wang, and M. Huang, "Up to the 1552nd order passively harmonic mode-locked Raman fiber laser," IEEE Photon. Technol. Lett. **27**, 2205 (2015).
47. G. P. Agrawal, in Nonlinear Fiber Optics (Fifth Edition) (Elsevier Inc., 2013).
48. N. J. Doran and D. Wood, "Nonlinear-optical loop mirror," Opt. Lett. **13**, 56 (1988).